Color Figures for the Article

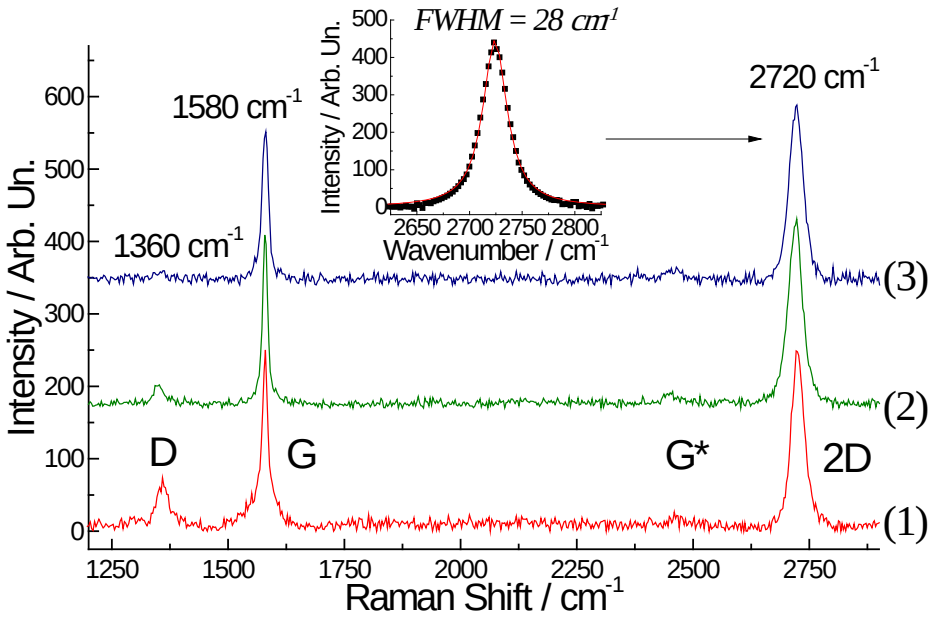

Figure 1. Raman spectra of graphene obtained at hydrogen flow rate (1) *150 cc/min*, (2) *60 cc/min* and (3) in the absence of hydrogen. Inset: approximation of 2D peak by a single Lorentz function.

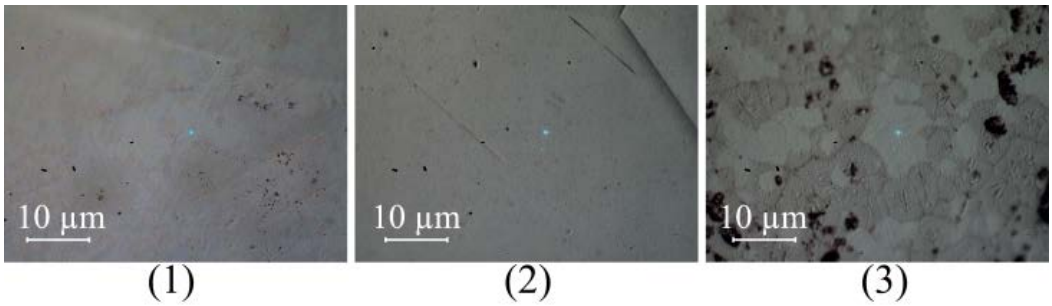

Figure 2. Optical microscope images (zoom 100×) of graphene obtained at hydrogen flow rate (1) *150 cc/min*, (2) *60 cc/min* and (3) in the absence of hydrogen.

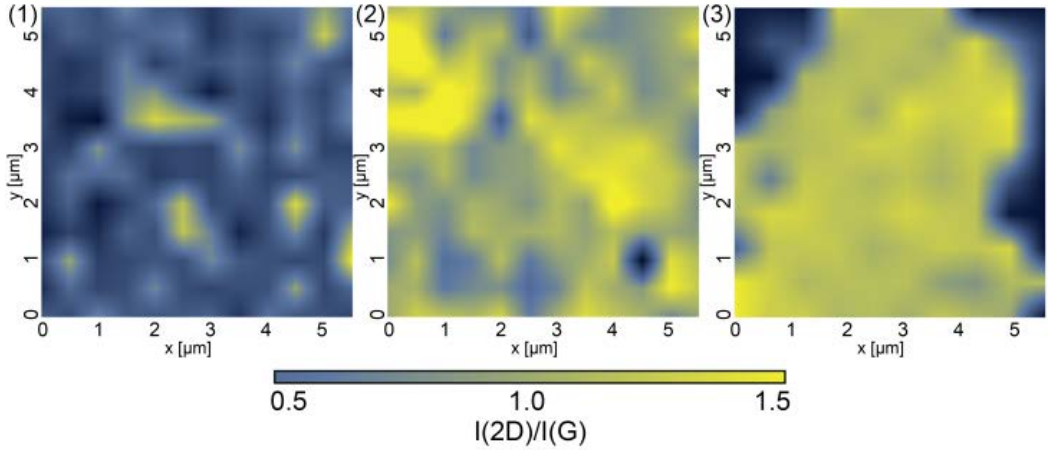

Figure 3. Raman maps (5×5 µm) of the intensity ratio I(2D)/I(G) for graphene obtained at hydrogen flow rate (1) *150 cc/min*, (2) *60 cc/min* and (3) in the absence of hydrogen; scanning step of *0.4 µm*.

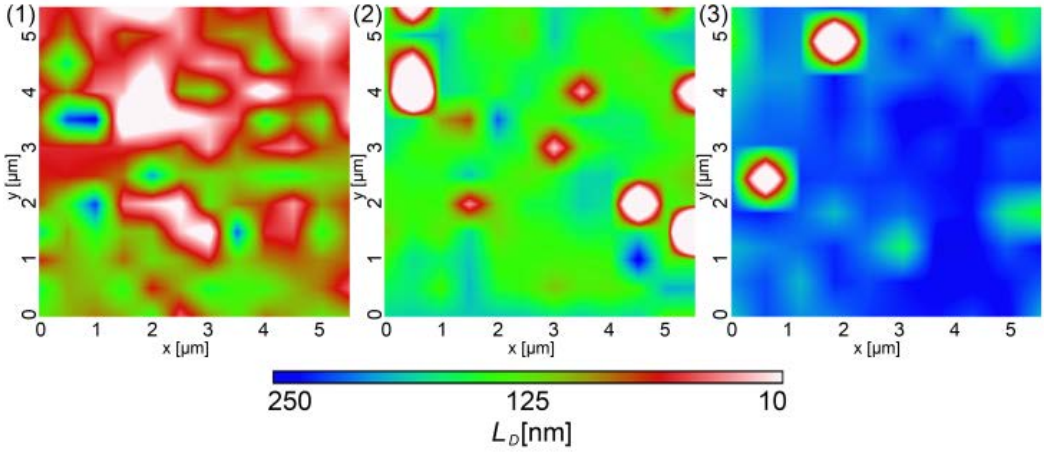

Figure 4. Raman maps (5×5 μm) of the average inter-defect distance for graphene obtained at hydrogen flow rate (1) *150 cc/min*, (2) *60 cc/min* and (3) in the absence of hydrogen; scanning step of *0.4 μm*.

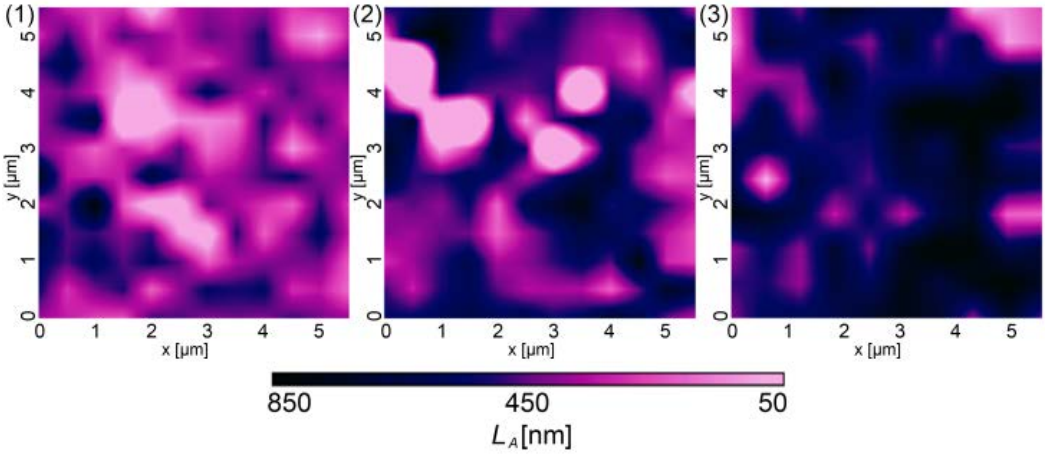

Figure 5. Raman maps (5×5 μm) of the average grain sizes for graphene obtained at hydrogen flow rate (1) *150 cc/min*, (2) *60 cc/min* and (3) in the absence of hydrogen; scanning step of *0.4 μm*.

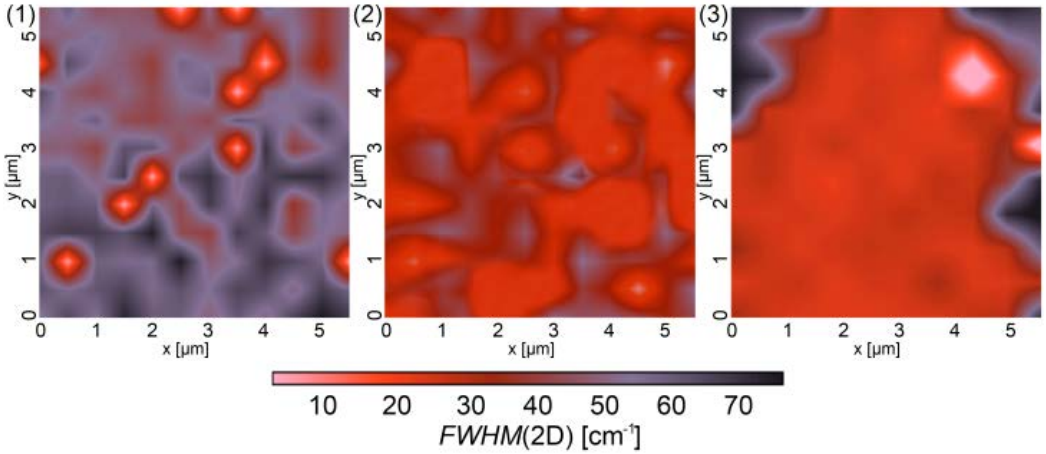

Figure 6. Raman maps (5×5 μm) of the *FWHM*(2D) for graphene obtained at hydrogen flow rate (1) *150 cc/min*, (2) *60 cc/min* and (3) in the absence of hydrogen; scanning step of *0.4 μm*.

DOI 10.1007/s10812-018-0574-z
Journal of Applied Spectroscopy, Vol. 84, No. 6, January, 2018 (Russian Original Vol. 84, No. 6, November–December, 2017)

RAMAN SPECTRA OF GRAPHENE SYNTHESIZED BY CHEMICAL VAPOR DEPOSITION FROM DECANE

M. S. Tivanov,[a] E. A. Kolesov,[a] O. V. Korolik,[a] A. M. Saad,[b] N. G. Kovalchuk,[c] I. V. Komissarov,[c] V. A. Labunov,[c] M. Opielak,[d] P. Zukowski,[e] and T. N. Koltunowicz[e]*

UDC535.375.5

Raman spectroscopy was used to study the structural properties of graphene synthesized by chemical vapor deposition using decane ($C_{10}H_{22}$) as a precursor at various hydrogen concentrations. Reduction of the carrier gas flow rate from 150 cm^3/min to zero changes the average spacing between the defects from 53 to 212 nm and the average grain size from 87 to 798 nm and changes the uniformity and continuity of the graphene layer. The obtained relationships can be used to control the defectiveness, homogeneity, and continuity of the graphene layer of the coating during synthesis by this method.

Keywords: graphene, chemical vapor deposition, decane, Raman spectroscopy, defect.

Introduction. The importance of research into graphene arises from its unique characteristics. Graphene is a promising material for various applications on account of its optical transparency, high mechanical strength, and thermal and electric conductivity [1–5]. It is at present being used in the production of field-effect transistors, biosensors, and transparent electrodes.

One of the most widely used methods of synthesis of graphene is chemical vapor deposition (CVD) [6–11]. By CVD it is possible to synthesize large areas of graphene that can then be transferred to other surfaces [12]. The synthesis of graphene with methane (CH_4) as precursor has been widely represented in the literature. The usual method of CVD synthesis of graphene on a catalyst substrate involves several stages [7] that depend to a significant degree on the type of precursor [11]. By using other hydrocarbons with different molecular mass as precursors it is possible to control the synthesis more effectively on account of change in the kinetics of growth of the graphene [11, 13].

Decane ($C_{10}H_{22}$) is a member of the homologous series of alkanes. In the present work the possibility of using it as precursor for the synthesis of graphene was investigated. We draw attention particularly to the following feature of the precursor. Thermal decomposition of decane is accompanied by the formation of $*C_xH_y$ radicals [14], the presence of which in the gas mixture reduces the dissociation energy of the bond in the nitrogen molecule [15, 16]. This leads to a larger concentration of nitrogen atoms in the gas mixture compared with the process that only involves thermal decomposition of the nitrogen molecules (bond energy 226 kcal/mole). This feature makes it possible to dope the graphene with nitrogen during the synthesis processes with decane as precursor and nitrogen as carrier [17]. All this gives rise to the need to study the processes involved in the synthesis of graphene from decane.

Another important reagent in the synthesis of graphene is hydrogen, which is not only used for the reduction of copper oxide on the surface of the catalyst [18] but also has a direct effect on the formation of graphene. During the growth of graphene in the presence of hydrogen the latter is adsorbed on the surface of the copper [19, 20]. The adsorbed hydrogen atoms act as co-catalyst in the decomposition of the hydrocarbon [21], and at low concentrations of hydrocarbon in the absence of H_2 the endothermic decomposition reaction takes places slowly. Moreover, the hydrogen removes surplus layers of graphene from the substrate [21, 22]. At the same time negative effects from the use of hydrogen in the synthesis

*To whom correspondence should be addressed.

[a]Belarusian State University, 220030, Minsk, Belarus; [b]Al-Balqa Applied University, PO Box 4545, Amman 11953, Jordan; [c]Belarusian State University of Informatics and Radioelectronics, 220013, Minsk, Belarus; [d]The State School of Higher Education in Chelm, 22-100 Chelm, Poland; [e]Lublin University of Technology, 38d Nadbystrzycka Str., 20-618 Lublin, Poland; email: t.koltunowicz@pollub.pl. Translated from Zhurnal Prikladnoi Spektroskopii, Vol. 84, No. 6, pp. 898–904, November–December, 2017. Original article submitted January 23, 2017.

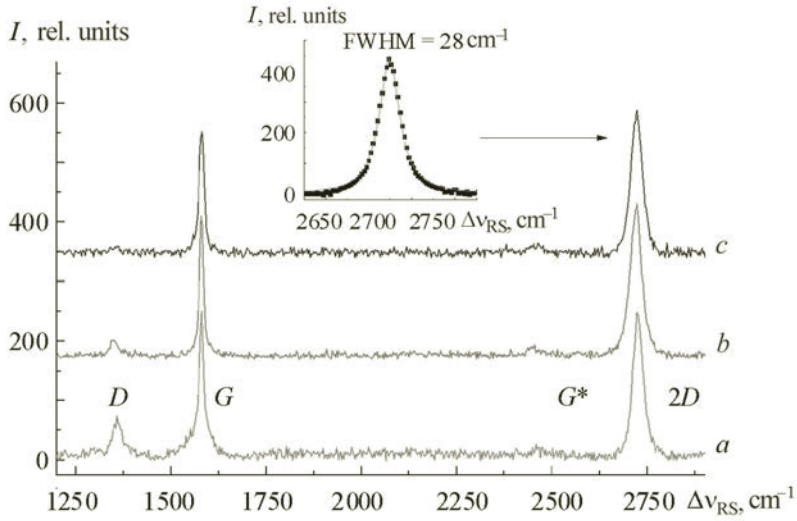

Fig. 1. Raman spectra of graphene produced with hydrogen consumption rates 150 (a) and 60 cm^3/min (b) and in the absence of hydrogen (c). Inset: approximation of 2*D* line by single Lorentz function.

of graphene with CH_4 have been reported in some papers, such as blockage of the surface of the substrate by the adsorbed hydrogen, preventing transfer of the hydrocarbon groups, etc. [23–25]. Such effects can lower the quality of obtained material when the graphene is produced from $C_{10}H_{22}$. Thus, the effect of hydrogen on the synthesis of graphene by CVD with decane as precursor requires further investigation.

The aim of the present work was to investigate the structural characteristics of graphene synthesized by CVD on copper with hydrogen at various concentrations and with decane as precursor by Raman spectroscopy [26, 27].

Experimental. The samples of the graphene structures were synthesized by CVD at atmospheric pressure. A copper foil 100-μm-thick and 99.9% pure was used as catalyst support. The support was first treated by electropolishing in a 1 M solution of phosphoric acid at a working potential of 2.3 V. The synthesis was conducted in a tubular quartz reactor with a diameter of 14 mm. Just before the synthesis the substrate was baked at 1050°C in an atmosphere of hydrogen (150 cm^3/min) and nitrogen (100 cm^3/min) for 60 min in order to remove copper oxides from the surface. The synthesis was realized at H_2 consumption rates of 150 and 60 cm^3/min and in the absence of hydrogen with other conditions equal: temperature 1050°C, $C_{10}H_{22}$ 30 μL/min, N_2 100 cm^3/min, synthesis time 10 min. After the hydrocarbon gas flow had stopped the sample was cooled to room temperature at a rate of ~50°C/min.

The Raman spectra and optical images were obtained on a confocal Nanofinder HE (LOTIS TII) spectrometer. Excitation was realized with the emission from a solid-state laser in continuous mode with wavelength 473 nm and optical power ~2.4 mW. The laser emission was focused on the surface of the sample in a spot with diameter ~0.6 μm. The Raman spectra were recorded in the region of 1000–3000 cm^{-1} at a spectral resolution no lower than 3 cm^{-1}.

The characteristic Raman lines of graphene were analyzed, i.e., the strongest *G* and 2*D* lines [28, 29] and also the *D* line characteristic of sp^2 carbon in the presences of defects [30]. The number of graphene layers was estimated from the ratio of the maximum intensities of the lines $I(2D)/I(G)$ and the full width of the 2*D* line at half maximum (FWHM) [31, 32]. The imperfection of the graphene was determined from the maximum intensity ratio of the lines $I(D)/I(G)$ [33]. The mean diameters of the graphene grains were calculated from the ratio of the integral areas under the lines $S(D)/S(G)$ [30, 34].

Results and Discussion. Figure 1 shows the characteristic Raman spectra of graphene synthesized with H_2 at 150 and 60 cm^3/min and in the absence of hydrogen. The calculated intensity ratios $I(2D)/I(G)$ and $I(D)/I(G)$ and FWHM(2*D*) are presented in Table 1.

The presence of a monolayer of graphene is confirmed by the FWHM(2*D*) values and also by the approximation of the 2*D* line by a single Lorentz function (Fig. 1, inset) [31, 32]. The $I(2D)/I(G) \sim 1$ ratios may be due to the presence of defects in the graphene [35, 36]. Increase of the $I(D)/I(G)$ ratio with increase of the hydrogen consumption indicates increased imperfection in the graphene [33].

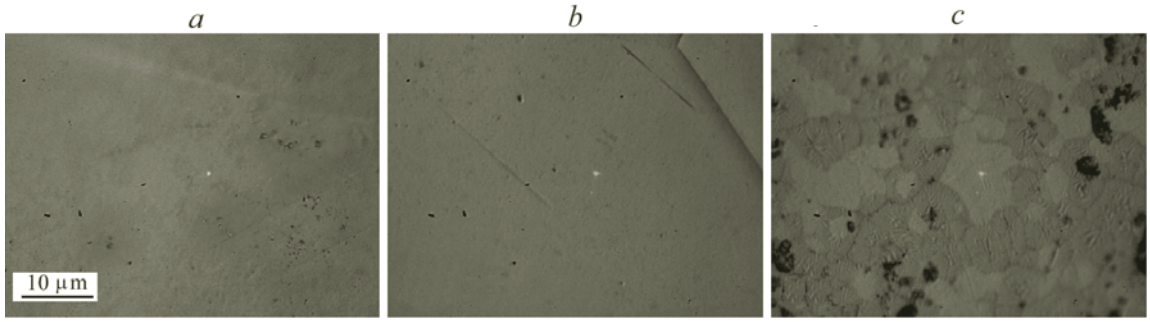

Fig. 2. Optical images of the surface (100×) of graphene produced with hydrogen at 150 (a) and 60 (b) cm^3/min of hydrogen and in the absence of hydrogen (c).

TABLE 1. Parameters of the Investigated Samples Calculated from the Raman Spectra

Hydrogen consumption rate, cm^3/min	150	60	0
$I(2D)/I(G)$	0.70	1.03	1.09
$I(D)/I(G)$	0.41	0.20	0.09
FWHM(2D), cm^{-1}	42	33	28
$\langle L_D \rangle$, nm	53 ± 12	117 ± 18	212 ± 29
$\langle L_A \rangle$, nm	87 ± 19	162 ± 24	798 ± 38

Figure 2 shows optical images of the surface of graphene synthesized with hydrogen at 150 and 60 cm^3/min and in the absence of hydrogen. It is seen that the surface of the samples obtained in the presence of hydrogen has a high degree of uniformity, whereas the surface of the sample synthesized without the use of H_2 is nonuniform.

Figure 3a shows the Raman map corresponding to the $I(2D)/I(G)$ ratio for the sample obtained with the highest hydrogen consumption. It is seen that the regions corresponding to several graphene layers ($I(2D)/I(G) < 1$) alternate randomly with regions where $I(2D)/I(G) > 1$. Here, the area of monolayer coating is insignificant. A different situation is observed for the sample synthesized with 60 cm^3/min of H_2 (Fig. 3b): the degree of coverage by sections with $I(2D)/I(G) > 1$ is substantially higher. The Raman map for the sampled synthesized in the absence of hydrogen (Fig. 3c) shows that $I(2D)/I(G) > 1$ for the greater part of the scanned region. At the same time there are regions where a graphene coating is not observed (the parameters of the Raman lines correspond to graphite), leading to a flaky structure in the graphene coating.

The average distance between the defects in the region of the laser spot L_D (nm) was calculated from the ratio of the maximum intensities of the D and G lines [33]:

$$L_D^2 = \frac{4.3 \cdot 10^3}{E_L^4} \left(\frac{I(D)}{I(G)} \right)^{-1},$$

where E_L is the laser excitation energy, eV.

Since the $I(2D)/I(G)$ does not depend on the geometry of the defects the calculated L_D values include all the Raman-active defects [37].

The Raman maps of L_D for the investigated samples are shown in Fig. 4. As seen, the distance between the defects increases with decrease of hydrogen consumption rate, and the distribution of this parameter here in the scanned region in Fig. 4b and c is relatively uniform. Despite the flaky structure of the coating a low degree of imperfection is observed for the graphene synthesized in the absence of hydrogen. The $\langle L_D \rangle$ values averaged over all the obtained spectra (144 spectra for each map) are presented in Table 1.

The average grain size L_A (nm) was calculated from the ratio of the areas under the D and G lines [30, 34]:

$$L_A = 2.4 \cdot 10^{-4} \lambda_L^4 [S(D)/S(G)]^{-1},$$

where λ_L is the excitation wavelength, nm; $S(D)$ and $S(G)$ are the areas under the D and G lines.

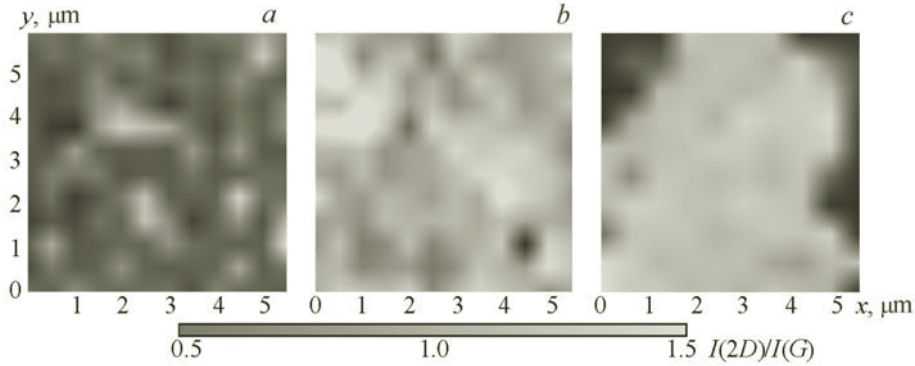

Fig. 3. Raman maps (5 × 5 μm) of the line intensity ratios $I(2D)/I(G)$ of graphene produced with 150 (a) and 60 cm^3/min (b) of hydrogen and in the absence of hydrogen (c); the scanning step was 0.4 μm.

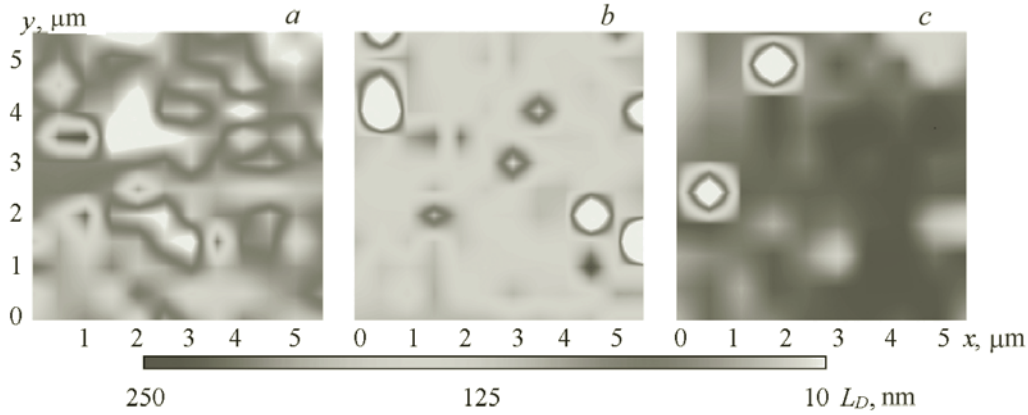

Fig. 4. Raman maps (5 × 5 μm) of the average distance between the defects in graphene produced with 150 (a) and 60 cm^3/min (b) of hydrogen and in the absence of hydrogen (c); scanning step 0.4 μm.

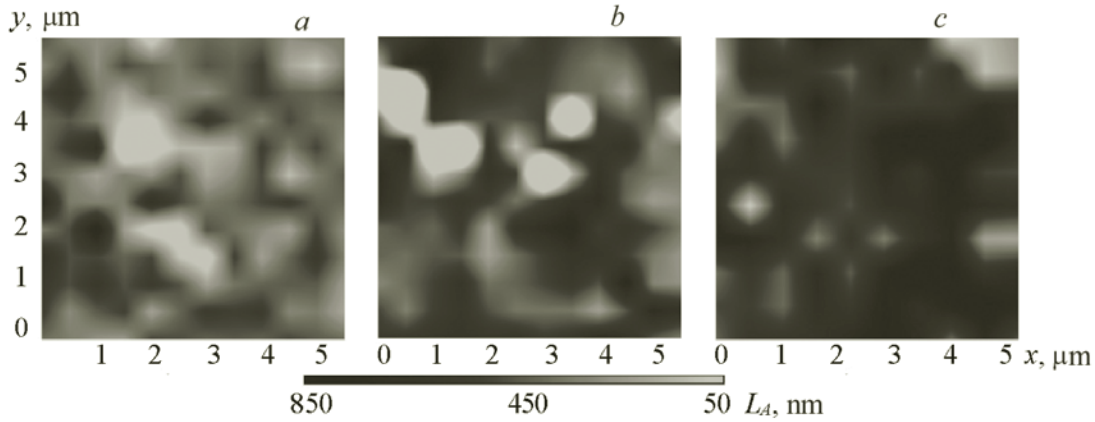

Fig. 5. Raman maps (5 ×5 μm) of the average grain sizes of graphene produced with 150 (a) and 60 cm^3/min (b) and in the absence of hydrogen (c); scanning step 0.4 μm.

The distribution maps of L_A correlate with the analogous distribution maps of L_D (Figs. 4 and 5). The proportion of relatively large grains (up to 850 nm) increases with decrease of the hydrogen consumption rate. The results of the calculations, averaged among all the points for each map ($\langle L_A \rangle$), are presented in Table 1.

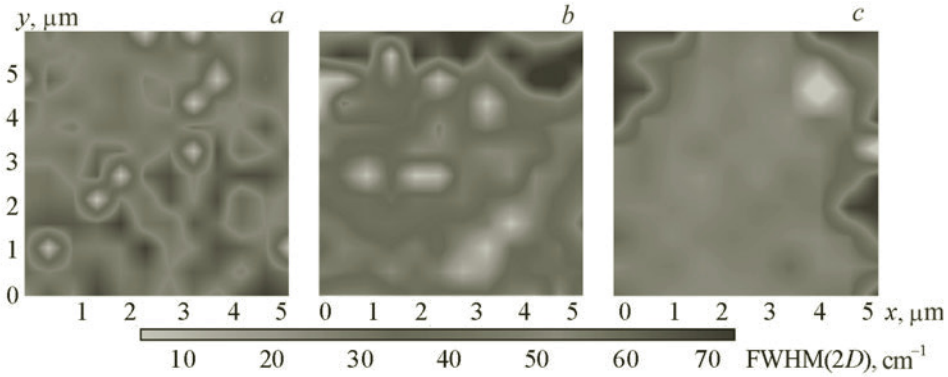

Fig. 6. Raman maps (5 × 5 μm) of FWHM(2*D*) for graphene obtained with 150 (a) and 60 cm^3/min (b) and in the absence of hydrogen (c); scanning step 0.4 μm.

Figure 6 shows the FWHM(2*D*) maps for the investigated samples. As seen, values corresponding to a single layer of graphene (<30 cm^{-1}) are present in Fig. 6b and c [32].

The variation of the average distance between the defects and the grain size of the obtained graphene with variation of the hydrogen consumption rate can be explained by several reasons. During decomposition and adsorption of the hydrocarbon on the surface of the substrate the process can compete with the dissociative chemisorption of hydrogen [22]. With a high H_2 consumption rate it blocks the substrate surface, preventing uniform adsorption of the hydrocarbon groups on the substrate [23, 24]. These processes can lead to the formation and growth of individual grains. At the growth stage the graphene layer is passivated by the copper surface, which prevents the growth of successive layers; here the strong adsorption of the hydrocarbon groups and carbon monomers extends to the boundary layer [38]. Hydrogen can reduce the degree of passivation, leading to the growth of successive layers. The dependence of the defectiveness of the graphene on the hydrogen consumption rate may arise from the formation of sp^3-hybridized CH bonds in the synthesis process [22], where their amount in the resultant material increases with increase of the hydrogen consumption rate. The bonds that form act as point defects. In addition, decrease of the average grain size with increase of the hydrogen consumption rate also leads to increase in the concentration of defects per unit surface of the synthesized material.

At 1000°C the solubility of hydrogen in copper amounts to 0.007 at.%. After cooling to room temperature the solubility falls to ~10^{-7} at.% [39]. At the cooling stage hydrogen can thus escape to the surface of the substrate, leading to the formation of additional defects in graphene that is produced with the use of hydrogen [25].

We discussed a possible mechanism for the effect of the hydrogen concentration in [17], where it was shown that decrease of the hydrogen concentration leads to the formation of more uniform graphene. Nevertheless, in the experiment without injected hydrogen the morphology of the sample becomes similar to the sample produced with a higher hydrogen consumption rate. This fact can be explained as follows. As discussed in [17], the hydrogen concentration (the partial pressure in the gas mixture) is a factor that determines the chain of reactions along which the decane decomposes. It can be supposed that the decomposition of decane in the absence of injected hydrogen occurs along a path in which the final decomposition products contain enough hydrogen for the formation of CH bonds at the edges of the graphene [38]. This leads to the result that the formation of such bonds, according to [38], becomes energetically favorable for the adsorbed carbon atoms.

Thus, the absence of H_2 as the reason for the formation of defects in the synthesis process reduces the imperfection of the graphene. At the same time, without hydrogen as co-catalyst the endothermic decomposition reactions of the hydrocarbons are retarded [21], which leads to the flaky structure of the synthesized material.

Conclusions. The graphene synthesized on copper foil by chemical vapor deposition from decane with various amounts of hydrogen was investigated by Raman spectroscopy. It was found that if the hydrogen consumption is reduced from 150 cm^3/min to zero the average distances between the defects are increased (from ~50 to ~200 nm) and the grain sizes of the synthesized graphene are increased (from ~90 to ~800 nm); the degree of coverage of the substrate with a monolayer of graphene is lowest in the case of synthesis without hydrogen. This effect may be due to competition between the two functions of the hydrogen: as one of the adsorbates and as catalyst in the synthesis of graphene. Hydrogen is thus essential for the synthesis of high-grade continuous films of graphene from decane, and its consumption rate for the reactor geometry used

in the present work must be less than 60 cm^3/min. Selection of the optimum consumption of hydrogen (small but not zero) is an important practical factor in the synthesis of high-grade uniform graphene from decane.

Acknowledgments. The work was supported by the State Program of Scientific Investigations of the Republic of Belarus (Photonics and Opto- and Microelectronics) and of the Scientific Research Fund of the Electrotechnology and Informatics Faculty of Lublin University of Technology, 8620/E-361/S/2016 (S-28/E/2016).

REFERENCES

1. H. G. Craighead and P. L. McEuen, *Science*, **315**, 490–493 (2007).
2. A. A. Balandin, S. Ghosh, W. Bao, I. Calizo, D. Teweldebrhan, F. Miao, and C. N. Lau, *Nano Lett*., **8**, 902–907 (2008).
3. K. I. Bolotin, K. J. Sikes, Z. Jiang, M. Klima, G. Fudenberg, J. Hone, Ph Kim, and H. L. Stormer, *Solid State Commun*., **146**, 351–355 (2008).
4. K. S. Novoselov, A. K. Geim, S. V. Morozov, K. S. D. Jiang, Y. Zhang, S. A. Dubonos, I. V. Grigorieva, and A. A. Firsov, *Science*, **306**, 666–669 (2004).
5. H. C. Cheng, R. J. Shiue, C. C. Tsai, W. H. Wang, and Y. T. Chen, *ACS Nano*, **5**, 2051–2059 (2011).
6. P. W. Sutter, J.-I. Flege, and E. A. Sutter, *Nat. Mater*., **7**, 406–411 (2008).
7. S. Bhaviripudi, X. Jia, M. S. Dresselhaus, and J. Kong, *Nano Lett*., **10**, 4128–4133 (2010).
8. J. Coraux, T. N. Plasa, C. Busse, and T. Michely, *New J. Phys*., 10043033 (2008).
9. S. Y. Kwon, C. V. Ciobanu, V. Petrova, V. B. Shenoy, J. Bareno, V. Gambin, I. Petrov, and S. Kodambaka, *Nano Lett*., **9**, 3985–3990 (2009).
10. A. Reina, S. Thiele, X. T. Jia, S. Bhaviripudi, M. S. Dresselhaus, J. A. Schaefer, and J. Kong, *Nano Res*., **2**, 509–516 (2009).
11. W. Song, C. Jeon, S. Y. Kim, Y. Kim, S. H. Kim, S. I. Lee, D. S. Jung, M. W. Jung, K. S. An, and C. Y. Park, *Carbon*, **68**, 87–94 (2014).
12. S. Bae, H. Kim, Y. Lee, X. Xu, J. S. Park, Y. Zheng, J. Balakrishnan, T. Lei, H. R. Kim, Y. I. Song, and Y. J. Kim, *Nat. Nanotech*., **5**, 574–578 (2010).
13. I. V. Komissarov, N. G. Kovalchuk, E. A. Kolesov, M. S. Tivanov, O. V. Korolik, A. V. Mazanik, Yu. P. Shaman, A. S. Basaev, V. A. Labunov, S. L. Prischepa, N. I. Kargin, R. V. Ryzhuk, and S. A. Shostachenko, *Phys. Proc*., **72**, 450–454 (2015).
14. J. M. Lemieux, *Thermal Decomposition of Molecules Relevant to Combustion and Chemical Vapor Deposition by Flash Pyrolysis Time-of-Flight Mass Spectrometry*, PhD Thesis, University of Riverside, Riverside, CA, USA (2013).
15. C. P. Fenimore, *Proc. Int. Symp. Combust.*, **13**, 373–380 (1971).
16. R. T. Bise, H. Choi, and D. M. Neumark, *J. Chem. Phys*., **111**, 4923–4932 (1999).
17. I. V. Komissarov, N. G. Kovalchuk, V. A. Labunov, K. V. Girel, O. V. Korolik, M. S. Tivanov, A. Lazauskas, M. Andrulevičius, T. Tamulevičius, V. Grigaliūnas, Š. Meškinis, S. Tamulevičius, and S. L. Prischepa, *Beilstein J. Nanotechnol.*, **8**, 145–158 (2017).
18. K. Celebi, *Chemical Vapor Deposition of Graphene on Copper*, PhD Thesis, Swiss Federal Institute of Technology, Zurich, Switzerland (2013).
19. A. Gelb and M. Cardillo, *Surf. Sci*., **59**, 128–140 (1976).
20. A. Gelb, *Surf. Sci*., **64**, 197–208 (1977).
21. I. Vlassiouk, M. Regmi, P. Fulvio, S. Dai, P. Datskos, G. Eres, and S. Smirnov, *ACS Nano*, **5**, 6069–6076 (2011).
22. M. Losurdo, M. M. Giangregorio, P. Capezzuto, and G. Bruno, *Phys. Chem. Chem. Phys*., **13**, 20836–20843 (2011).
23. J.-W. Snoeck, G. F. Froment, and M. Fowles, *J. Catal*., **169**, 240–249 (1997).
24. A. Becker, Z. Hu, and K. J. Huttinger, *Fuel*, **79**, 1573–1580 (2000).
25. S. Garaj, W. Hubbard, and J. A. Golovchenko, *Appl. Phys. Lett*., **97**, 183103 (2010).
26. L. M. Malard, J. Nilsson, D. C. Elias, J. C. Brant, F. Plentz, E. S. Alves, A. C. Neto, and M. A. Pimenta, *Phys. Rev. B*, **76**, 201401(R) (2007).
27. M. S. Dresselhaus, A. Jorio, M. Hofmann, G. Dresselhaus, and R. Saito, *Nano Lett*., **10**, 751–758 (2010).
28. A. C. Ferrari, J. C. Meyer, V. Scardaci, C. Casiraghi, M. Lazzeri, F. Mauri, S. Piscanec, D. Jiang, K. S. Novoselov, S. Roth, and A. K. Geim, *Phys. Rev. Lett*., **97**, 187401 (2006).
29. R. P. Vidano, D. B. Fischbach, L. J. Willis, and T. M. Loehr, *Solid State Commun*., **39**, 341–344 (1981).

30. F. Tuinstra and J. Koenig, *J. Chem. Phys.*, **53**, 1126–1130 (1970).
31. A. C. Ferrari and D. M. Basko, *Nat. Nanotech.*, **8**, 235–246 (2013).
32. Y. Hao, Y. Wang, and L. Wang, *Small*, **6**, 195–200 (2010).
33. L. G. Cançado, A. Jorio, E. M. Ferreira, F. Stavale, C. A. Achete, R. B. Capaz, M. V. O. Moutinho, A. Lombardo, T. S. Kulmala, and A. C. Ferrari, *Nano Lett.*, **11**, 3190–3196 (2011).
34. L. G. Cançado, K. Takai, T. Enoki, M. Endo, Y. A. Kim, H. Mizusaki, N. L. Speziali, A. Jorio, and M. A. Pimenta, *Carbon*, **46**, 272–275 (2008).
35. E. H. Hasdeo, A. R. T. Nugraha, M. S. Dresselhaus, and R. Saito, *Fermi Energy Dependence of First- and Second-Order Raman Spectra in Graphene: Kohn Anomaly and Quantum Interference Effect*, arXiv:1605.02837 (2016).
36. M. Bruna, A. K. Ott, M. Ijäs, D. Yoon, U. Sassi, and A. C. Ferrari, *ACS Nano*, **8**, 7432–7441 (2014).
37. A. Eckmann, A. Felten, and A. Mishchenko, *Nano Lett.*, **12**, 3925–3930 (2012).
38. X. Zhang, L. Wang, J. Xin, B. I. Yakobson, and F. Ding, *J. Am. Chem. Soc.*, **136**, 3040–3047 (2014).
39. E. Fromm and H. Jehn, *Bull. Alloy Phase Diagram*, **5**, 324–326 (1984).